Deep-Sea Research II 85 (2013) 154–168

Contents lists available at SciVerse ScienceDirect

Deep-Sea Research II

journal homepage: www.elsevier.com/locate/dsr2

Variability of the Deep Western Boundary Current at 26.5°N during 2004–2009

Christopher S. Meinen*, William E. Johns, Silvia L. Garzoli, Erik van Sebille, Darren Rayner, Torsten Kanzow, Molly O. Baringer

NOAA/AOML/PHOD, 4301 Rickenbacker Causeway, Miami, FL 33149, United States

ARTICLE INFO

Available online 3 August 2012

Keywords:
Meridional Overturning Circulation
Deep Western Boundary Current
Transport
Inverted Echo Sounder
Thermohaline
Variability

ABSTRACT

Five years of data from a line of dynamic height moorings (DHM), bottom-pressure recorders (BPR), and pressure-equipped inverted echo sounders (PIES) near the Atlantic Ocean western boundary at 26.5°N are used to evaluate the structure and variability of the Deep Western Boundary Current (DWBC) during 2004–2009. Comparisons made between transports estimated from the DHM+BPR and those made by the PIES demonstrate that the two systems are collecting equivalent volume transport information (correlation coefficient $r=0.96$, root-mean-square difference=6 Sv; 1 Sv=10^6 m^3 s^{-1}). Integrated to ~450 km off from the continental shelf and between 800 and 4800 dbar, the DWBC has a mean transport of approximately 32 Sv and a standard deviation during these five years of 16 Sv. Both the barotropic (full-depth vertical mean) and baroclinic flows have significant variability (changes exceeding 10 Sv) on time scales ranging from a few days to months, with the barotropic variations being larger and more energetic at all time scales. The annual cycle of the deep transport is highly dependent on the horizontal integration distance; integrating ~100 km offshore yields an annual cycle of roughly similar magnitude but shifted in phase relative to that found from current meter arrays in the 1980–1990s, while the annual cycle becomes quite weak when integrating ~450 km offshore. Variations in the DWBC transport far exceed those of the total basin-wide Meridional Overturning Circulation (standard deviations of 16 Sv vs. 5 Sv). Transport integrated in the deep layer out to the west side of the Mid-Atlantic Ridge still demonstrates a surprisingly high variance, indicating that some compensation of the western basin deep variability must occur in the eastern basin.

Published by Elsevier Ltd.

1. Introduction

Variations of the Meridional Overturning Circulation (MOC) in the Atlantic Ocean have been correlated in numerical model simulations with changes in precipitation, surface air temperature, hurricanes and other crucially important quantities for society (e.g. Stouffer et al., 2006; Vellinga and Wood, 2002; Zhang and Delworth, 2006). As understanding of the importance of the MOC has grown over the past few years, increased resource commitment has led to an improving picture of the MOC system through programs like the trans-basin MOC monitoring array at 26.5°N that started in 2004 (e.g. Cunningham et al., 2007; Johns et al., 2008, 2011; Kanzow et al., 2007; Rayner et al., 2011).

The Deep Western Boundary Current (DWBC), first hypothesized by Stommel (e.g. Stommel, 1957; Stommel and Arons, 1960) and first measured by Swallow (e.g. Swallow and Worthington, 1961), is thought to carry the bulk of the lower limb of the MOC as it transits along the eastern seaboard of the Americas from the high latitude North Atlantic Ocean to the Southern Ocean. While modern studies have been finding that the flow of the DWBC may be less well confined to the continental slope than had previously been thought at locations such as 42°N (Bower et al., 2009) and 8–11°S (Dengler et al., 2004; Schott et al., 2005), at 26.5°N long-term measurements have demonstrated that the DWBC southward flow is reliably found along the continental slope (e.g. Hacker et al., 1996; Johns et al., 1997; Leaman and Harris, 1990; Lee et al., 1996; Molinari et al., 1992; Riser et al., 1978). Repeated hydrographic sections at this location have documented changes in the water masses being carried by the DWBC system from higher latitudes (e.g. Molinari et al., 1998; van Sebille et al., 2011), while moored observations have demonstrated a high degree of variability in the DWBC volume transports (e.g. Johns et al., 2005; Lee et al., 1996; Meinen et al., 2006).

Early study of the DWBC was mainly completed using Lagrangian floats, beginning with the Swallow float in the 1950–1970s (e.g. Swallow and Worthington, 1961; Riser et al., 1978), and such studies of the DWBC have continued to this day (e.g. Bower et al., 2009). These studies have provided important insights into the

* Corresponding author. Tel.: +1 305 361 4355; fax: +1 305 361 4412.
E-mail address: Christopher.Meinen@noaa.gov (C.S. Meinen).

0967-0645/$ - see front matter Published by Elsevier Ltd.
http://dx.doi.org/10.1016/j.dsr2.2012.07.036

structure, strength, pathways, and variability of the DWBC. Eulerian measurement systems have also provided crucial knowledge about the DWBC, particularly regarding the variability of its time scales and horizontal structure. While the DWBC has been studied via Eulerian mooring arrays at a variety of locations along its Atlantic path, including 42°N (e.g. Schott et al., 2004), 39°N (e.g. Joyce et al., 2005), 16°N (e.g. Kanzow et al., 2008), and 11°S (e.g. Schott et al., 2005), one of the longest observational records of the DWBC comes from 26.5°N. Routine study of the DWBC at 26.5°N began in 1984 when the Subtropical Atlantic Climate Studies (STACS) program expanded from the Straits of Florida out beyond the Bahamas Islands (Molinari et al., 1985; Molinari, 1986). Initially observations were collected solely using ship section data including CTD (e.g. Molinari et al., 1998) and Pegasus (e.g. Leaman and Harris, 1990), but in the late 1980s moorings were deployed to monitor hour-to-hour and day-to-day variations in the DWBC and they were maintained off and on until the late 1990s. A good review of the mooring studies of the DWBC east of the Bahamas between 1986 and 1997 can be found in Bryden et al. (2005a).

In 2004 the confluence of three programs led to what is arguably the most detailed observing system for the DWBC to date at 26.5°N. The NOAA Western Boundary Time Series (WBTS) project maintains both the long-term observations in the Florida Current in the Straits of Florida at 27°N (e.g. Larsen and Sanford, 1985; Meinen et al., 2010) as well as hydrographic observations of the Antilles Current and DWBC originally begun under STACS. In addition, in September 2004 the WBTS program deployed a set of pressure-equipped inverted echo sounders (PIES) along 26.5°N from the Bahamas out to 72°W to monitor changes in both the DWBC and the northward flowing Antilles Current (Meinen et al., 2006). At about the same time, in April 2004, a major new array of tall taut-line moorings was deployed across the entire basin from the Bahamas to Morocco along 24–26.5°N as part of the U.S. Meridional Overturning Circulation Heat-flux Array (MOCHA) and U.K. Rapid-Meridional Overturning Circulation (RAPID-MOC) programs (e.g. Cunningham et al., 2007; Johns et al., 2008; Kanzow et al., 2007). This trio of programs, coupled with satellite and model wind speed estimates, is providing the first trans-basin time series observations of the complete MOC; the programs are also providing what is probably the best resolution of DWBC observations ever obtained, using a variety of measurement systems. To date there are five years of DWBC and MOC observations from these systems, providing the opportunity to study time scales up to a few years as well as the relationship between the transport variability of the DWBC and that of the basin-wide MOC.

The purpose of this article is to present five years of detailed observations of DWBC volume transport variability from the combined WBTS/MOCHA/RAPID-MOC programs and to discuss the observed variability in the context of changes in the basin-wide MOC. Comparisons will be presented of the variations captured by different elements of the observing system, with discussion of the merits of the different systems and implications for further long-term monitoring of the DWBC. The results will also be compared to historical observations of the DWBC, made in the same region during the previous decades, to infer something about longer-time-scale variability.

2. Data and methods

The volume transports presented herein are based primarily on observations of full-water-column profiles of dynamic height anomaly as well as time series of bottom pressure measurements. Horizontal gradients in the former, determined between mooring sites, provide geostrophic relative velocity profiles, while horizontal gradients in the latter provide absolute geostrophic velocities at the bottom that can reference the relative velocity profiles. Two different measurement systems were utilized for both the dynamic height anomaly profile calculations and also for the bottom pressure measurements. Because most of the techniques utilized herein are well established, they will be reviewed only briefly, with the reader directed to the appropriate references for full details.

The first technique that is used for obtaining dynamic height anomaly profiles is based on the measurements of a 'dynamic height mooring' (DHM). Unlike the classical taut-line tall mooring with a series of current meters attached at different depths, the DHM has a series of temperature-conductivity-pressure recorders at a range of depths from nominally 100 m below the surface down to near the bottom—a 4500 m long mooring contains 15–25 recorders (e.g. Johns et al., 2005). Like any taut-line mooring, the DHM tends to 'blow-over' in strong currents, with maximum deflections/depth changes of 400+ m over the first five years of the MOCHA and RAPID-MOC experiment, so that data near the surface are occasionally missing. The data from the DHM sensors are interpolated vertically using a canonical $\delta T/\delta z(T)$ and temperature–salinity relationship derived from historical hydrography to obtain continuous temperature and salinity profiles at the mooring locations. The result is a full-water-column estimate of temperature, salinity and dynamic height anomaly at 20 m vertical resolution[1]; for details on the vertical interpolation and gridding procedure see Johns et al. (2005) and Kanzow et al. (2006).

The other technique used to estimate the full-water-column dynamic height anomaly is based on the measurements of an inverted echo sounder (IES). The IES measures round-trip acoustic travel time for 12 kHz signals (or 10 kHz in some older models) to travel up to the sea-surface and return (e.g. Rossby, 1969; Watts and Rossby, 1977). By combining the travel time measurements with 2-dimensional look-up fields of temperature and salinity, empirically derived from historical hydrography via the 'Gravest Empirical Mode' (GEM) method, the IES data can be used to provide time series estimates of temperature and salinity profiles over the full-water-column; for details on the GEM method and the application to IES data see Meinen and Watts (2000) and Watts et al. (2001).

Although two different instrument systems are collecting bottom pressure measurements in this experiment, the measurements themselves are essentially identical. At the base of each of the tall moorings deployed as part of MOCHA and RAPID-MOC is an additional small mooring with one or two bottom-pressure recorders (BPRs) mounted on a frame attached to an anchor. Meanwhile, each of the inverted echo sounders deployed as part of the WBTS program is also equipped with bottom pressure sensors (leading to them being referred to as PIES). The same type of Paros Scientific pressure sensor is used in the BPRs and the PIES—each is accurate to better than a hundredth of a decibar at time scales of a few days, however each system is also subject to exponential and/or linear drifts over the first few months (generally exponential) and over the full record (generally linear). More details on pressure gauge accuracy and drift can be found in Donohue et al. (2010) and Watts and Kontoyiannis (1990). In an effort to better understand and remove the pressure drift from these records, an overlapping deployment plan has been pursued between the joint programs at most of the sites with recovery and deployments staggered by at least six months between pairs of

[1] Note the DHM data utilize the canonical relationship only up to a depth of 100 m or the nominal depth of the shallowest sensor, whichever is shallower. For this study the data to the surface have been filled assuming a well-mixed upper layer.

instruments at each site. More detail on the drift removal and record merging of the pressure data is provided in the Appendix A.

Differencing neighboring pressure sensors provides a geostrophic estimate of the near-bottom velocity orthogonal to the line between them (in this case meridional velocity is obtained from the zonal line of moorings). However, because of the well-known 'leveling' problem associated with imprecise knowledge of the vertical distance of each sensor from a constant geopotential surface (e.g. Donohue et al., 2010), the pressure differences between sensors yield only an estimate of the absolute near-bottom geostrophic velocity *anomaly*, i.e. they provide no information on the time-mean near-bottom geostrophic velocity. This issue is addressed in the present study in two steps: first, the time mean velocities from historical near-bottom current meters deployed along the same line during the earlier STACS program and tabulated by Bryden et al. (2005a) are used. The mooring deployments ranged in length from 3 to 10 years, depending on the site (see Bryden et al., 2005a for details, also Lee et al., 1996). These time-mean historical current meter velocities are averaged horizontally between pairs of the modern mooring sites to provide an initial estimate of the time-mean near-bottom absolute reference velocity. Note that this estimate of the time-mean near-bottom absolute reference velocity may not be representative of the time-mean during the period of our study. Hence, the second step involves comparing the resulting absolute transport time series to the absolute transports estimated using data from ten ship sections along the array between 2004 and 2009 and adjusting the STACS-based initial estimate when transport differences exceeded some threshold (5 Sv). The processing steps to compute the absolute transports from the ten ship sections are given below. This adjustment resulted in changes to the absolute time mean velocity field of less than 5 cm s^{-1} (typically 1–2 cm s^{-1}), which then resulted in differences between the ten ship-sections and the absolute transport time series ranging from 2 to 5 Sv.

Absolute transports were calculated from the data collected on each of the ten ship sections in two ways: (1) from direct integration of both hull mounted Acoustic Doppler Current Profiler (ADCP) and lowered Acoustic Doppler Current Profiler (LADCP) data and (2) using conductivity–temperature–depth (CTD) station data referenced to the hull-mounted ADCP data. The first technique for calculating transport from the ship data is based on the straightforward integration of ADCP and LADCP data profiles between each mooring site (this method is referred to as ADCP+LADCP). The second method begins by computing geostrophic relative velocity profiles from CTD station data; these relative velocity profiles are then absolutely referenced using the direct velocity measurements made by the hull-mounted ADCP (this method is referred to as CTD+ADCP). The hull-mounted ADCP data is integrated horizontally between pairs of CTD sites and vertically from ~100 m down to the deepest common depth, typically 700–800 m, to create the absolute velocity reference for the CTD-derived geostrophic relative velocity profiles. The ADCP+LADCP derived transports gave similar values to the CTD+ADCP derived transports in all but one mooring span (the broad ~350 km span between Sites D and E/WB-5).

A third independent data set, data from the Argo float system, was investigated to see if absolute referencing of the 10 ship-based sections could be obtained through comparison with contemporaneous Argo velocities to possibly reconcile or replace the two referencing schemes described above. It was found that the spacing of nearly all the mooring pairs was so narrow that not enough Argo data exists for use in referencing. The one exception was in the broad ~350 km span between Sites D and E/WB-5, which as noted above was the only span where the merged LADCP+ADCP did not agree as well with the CTD+ADCP estimates. In this case the latter CTD+ADCP method was identified as 'better' because it agreed with the spatially-and-temporally averaged Argo velocities at 1000 dbar in that span.

Given the several Sv (1 Sv=10^6 m^3 s^{-1}) estimated accuracy of the section transports, agreement between the ship-section and mooring transports was only sought to within 2–5 Sv. In cases where the average of the ten section transports differed from the concurrent mooring transports by more than this threshold, small (order 1–5 cm s^{-1}) adjustments were made to the initial STACS current meter-based reference velocity estimate to reduce the transport offsets from the sections. Because of the inherent limitations of all methods of obtaining the time-mean near-bottom velocity, the time-mean transports presented herein should be considered with caution. Bias errors in the mean transports may be as high as ~2–3 Sv in the inshore segments of the DWBC array between sites B and D, and up to 5 Sv for the long span between sites D and E/WB-5 (see Figs. 1 and 2).

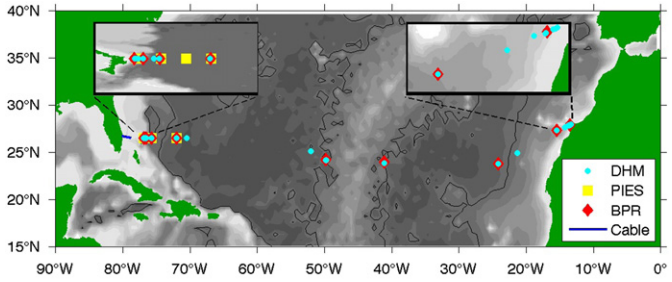

Fig. 1. Map with two zoomed insets illustrating the locations of the moorings associated with the collaborative WBTS, MOCHA, and RAPID-MOC programs. Yellow squares denote PIES, red diamonds denote BPR, and cyan circles denote taut-line moorings. Note that in some cases the moorings are deployed at essentially the same location at this scale (i.e. within 1 nm of one another), so the symbols overlay each other in those cases. Also shown (blue line) is the approximate location of the cable used for monitoring the Florida Current. Gray-scale denotes the bottom topography from Smith and Sandwell (1997) with 500 m contour levels, while green indicates land. The 4800 m contour is included for orientation as a thick black line.

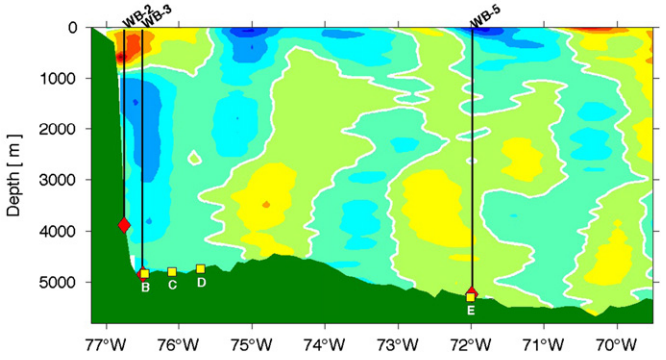

Fig. 2. Vertical section plot illustrating the locations of the moored instruments used herein for estimating the DWBC in relation to the bottom topography (green). PIES are denoted by yellow squares, bottom pressure sensors are shown as red diamonds, and tall moorings are indicated by vertical lines. Names for the tall moorings and bottom pressure recorders are noted along the top in black, while PIES names are denoted along the bottom in white. Contour field is meridional velocity (5 cm s^{-1} contour interval; zero contour in white) based on a crude smoothing of all historical velocity section data available with yellows and reds indicating northward flow and blues denoting southward flow. Velocity field is shown only to illustrate the relation of the sites to the flow—details of the flow should not be emphasized as the required smoothing applied was fairly strong.

Table 1
Longitudes (along 26° 30′N) where the WBTS, MOCHA, and RAPID-MOC moorings used to study the DWBC are located. Site on the western edge of the Mid-Atlantic Ridge (MAR-W) also indicated—note latitude for this site is 24° 10′N. Types of moorings include tall 'dynamic height' moorings (DHM), bottom pressure recorders (BPR), and pressure-equipped inverted echo sounders (PIES). The WB-2 and WB-3 moorings also carry some current meters as well as temperature-salinity-pressure recorders.

Site name	Type of mooring	Longitude
WB-2	DHM and 2 BPR	76° 44′W
WB-3	DHM and 1 BPR	76° 29′W
B	PIES	76° 28′W
C	PIES	76° 05′W
D	PIES	75° 42′W
E	PIES	72° 00′W
WB-5	DHM and 1 BPR	71° 59′W
MAR-W	DHM and 2 BPR	49° 43′W

The portion of the complete trans-basin array (Fig. 1) that is utilized for measuring the DWBC consists of three tall taut-line DHM[2] and four PIES.[3] The nominal longitudes of each mooring site are provided in Table 1 and are illustrated relative to a smoothed schematic of meridional velocity in Fig. 2. The locations of the PIES are based on the historical locations of moorings that were used in this region in the 1980s and 1990s (e.g. Bryden et al., 2005a; Lee et al., 1990, 1996). Typically the DWBC is located between the continental shelf and Site D, while between sites D and E a significant recirculation to the North is expected based on the earlier experiments (e.g. Chave et al., 1997; Lee et al., 1996). The WB-2 site was deployed to capture the flow located inshore of the B site, while the WB-3 and WB-5 sites were deployed to capture the 'net' DWBC transport after integrating out the recirculation.

The moored instruments are generally set to collect measurements at least once per hour. For this study all time series were low-pass filtered with a 72-h second-order Butterworth filter (passed both forward and backward to avoid phase shifting) and the resulting records were subsampled to once-per-day (noon UTC). Further details of the processing for the data collected by the instruments on the DHM followed the methods presented in Johns et al. (2008), while the PIES data were processed following the methods presented in Meinen et al. (2006).

3. Results

After processing, each mooring (DHM or PIES) provides daily time series of temperature, salinity, density, and dynamic height over the full water column at 20 dbar vertical resolution. Gradients from pairs of moorings, coupled with bottom pressure differences, provide full-water-column profiles of absolute meridional velocity each day. The time span of data that will be presented here is April 2004 through April 2009—note that due to equipment failure there are some time gaps at some of the sites. The transport of the DWBC will be determined via integration between 800 dbar and 4800 dbar as has been done in previous studies (e.g. Lee et al., 1996; Meinen et al., 2006). The mean and time varying results are not particularly sensitive to modest (~100–200 dbar) changes in the pressure levels which bound the integration.

[2] A fourth DHM has been deployed in the region but is not used herein due to the limited record resulting from instrument failures.

[3] Note that in two cases the PIES are co-located within one nautical mile of DHM.

3.1. Water property variations

Important results on the time scale of advective water-mass anomalies in the MOC system have come from the quasi-annual hydrographic sections collected along the so-called 'Abaco' line east of the Bahamas along 26.5°N since 1984 (e.g. Molinari et al., 1998; van Sebille et al., 2011). However, one thing that is clearly illustrated in recent moored observations is that water-mass variability in this region, and probably in many other places, is much greater than revealed by the available hydrographic sampling. The region east of Abaco is perhaps one of the most regularly sampled current regimes in the world, with more than 30 hydrographic sections collected since 1984 (e.g. Molinari et al., 1998; van Sebille et al., 2011). Nevertheless, the range of temperatures and salinities observed by the first five years of moored temperature and salinity observations well exceeds that of all of the existing hydrographic observations near the mooring sites (Fig. 3). This is particularly true in the main thermocline–halocline level, between roughly 300 dbar and 1000 dbar, where the range of observed temperature and salinity variability from the moorings is from 25% to more than 100% greater than the range of all hydrographic observations ever taken within 10 km of those locations, particularly at Site E/WB-5 where there are fewer historical CTD observations (57 casts at Site B/WB-3; 14 casts at Site E/WB-5). To determine whether the distributions of temperature and salinity profiles from the DHM were statistically distinct from those measured by the CTD data, a two-sample Kolmogorov–Smirnov test was completed (e.g. Van Sebille et al., 2009). The results suggest that the distributions are not distinct at

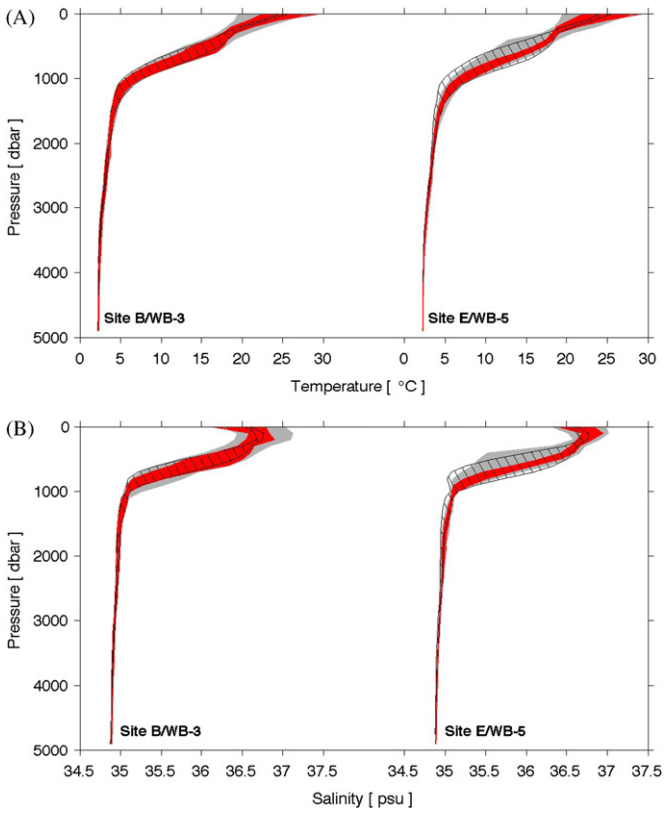

Fig. 3. Comparison between the temperatures (top panel) and salinities (lower panel) observed near the locations of Site B/WB-3 and Site E/WB-5 from the five years of tall-mooring data (gray), from the PIES data (cross-hatch), and from all hydrographic observations ever taken within 10 km of each site (red). The PIES data show significantly less variability in the upper 200–300 dbar because no seasonal corrections have been applied to the PIES-GEM data.

the 95% level, which indicates that the observed differences are not due to seasonal biasing or biases associated with the different types of sensors. The difference in observed temperature and salinity ranges therefore clearly illustrates the need to use caution when interpreting signals between different snapshot sections (e.g. Baringer and Molinari, 1999; Bryden et al., 2005b; Kanzow et al., 2010), as the differences may be based on fairly short time scale signals that are unrepresentative of longer-term changes.

As an example of this, in May–June 2006 there was an anomalous cold, fresh, event that occurred at Site E/WB-5 that brought waters that had never before been observed in this region (Fig. 4). This ~4 week event was centered between roughly 300 dbar and 1000 dbar, with temperature changes of around 5 °C and salinity changes of nearly 1 psu. It was observed in three different *T–S* sensors at different depth levels, so it was clearly not an instrumental problem. The event is clearly reproduced in the PIES measured travel time record at Site E as well (Fig. 5). The PIES-GEM estimated temperature and salinity profiles are based on the historical hydrographic database for the region (not just at the mooring sites; e.g. Meinen et al., 2006), so since this event is beyond the range of the existing hydrographic data it is also beyond the range of the 2-dimensional GEM look-up tables. However the modest extrapolation commonly used in building the GEM fields produces data that reproduces the measurements of the mooring during this event fairly well. Focusing on the travel time records (Fig. 5) to avoid concern regarding extrapolation of the GEM field, one finds that this event corresponded to an 8+ ms increase in travel time. Similar 6+ ms signals were observed at different times at Sites D, C, and B, however no consistent lag-pattern is found, indicating either that there is no zonal propagation of this or other similar events or that the features evolve sufficiently between sites that they cannot be tracked. An explanation for this event is beyond the scope of the present manuscript (preliminary comparison to climatology suggests a subpolar gyre origin) and will be addressed further in a future paper, however in the context of the present study it illustrates the significant aliasing that is possible through the use of snapshot sections as well as the need for continuous measurement systems to characterize the true range of signals that can be observed in this area.

3.2. Comparison of transports determined from DHM and from PIES

To obtain a full picture of the DWBC transport structure and variability it is crucial to utilize both the DHM and the PIES data in order to produce the best horizontal resolution of the signals (see Fig. 2). However, before combining the two different data sets it is important to demonstrate that the two systems are measuring the same thing. Based on the array designs (Fig. 2), the only pairs of moorings that can be used for a direct comparison are the DHM sites WB-3 and WB-5 and the PIES sites B and E. In comparing the absolute transports we note that the same blended bottom pressure records are used to reference both sets of relative velocity profiles, so they are not completely independent. Note also that at site B the PIES failed for a few months in mid-2006 and again in mid-2008 through 2009; also at site E and WB-5 bottom pressure data is not available for several months in mid-2008 due to multiple instrument failures.

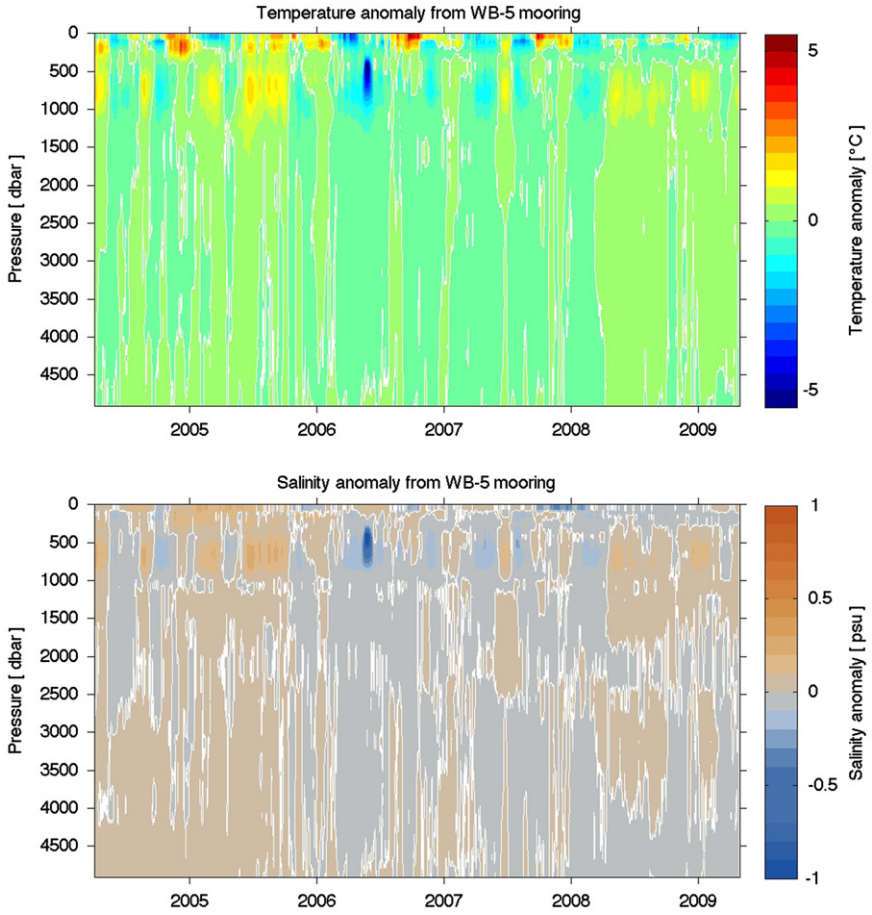

Fig. 4. Time series of profiles of temperature anomaly (upper panel) and salinity anomaly (lower panel) from the DHM site WB-5. Anomalies are calculated relative to the 5-year mean at each pressure.

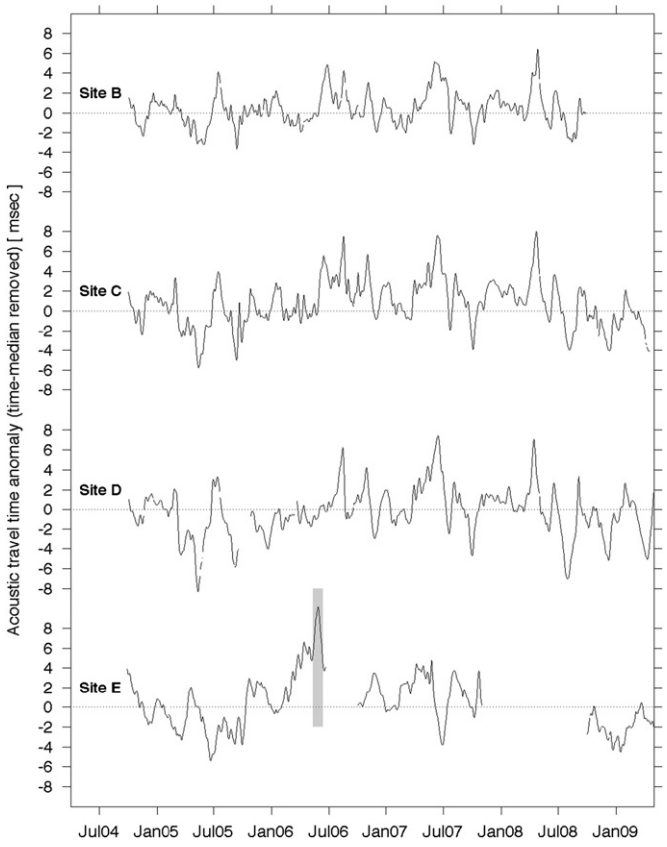

Fig. 5. Time series of acoustic round trip travel time measured by the PIES at the indicated sites (see Fig. 2 for site locations). Travel times shown are anomalies relative to the median for each site. Gray shading highlights the strong cold/fresh event discussed in the text. Gaps in records result from instrument failures.

Table 2
Percentages of DWBC transport variance (transport integrated from shelf to Site E/WB-5) observed within each time scale. Percentages were determined by low-pass, high-pass, or band-pass filtering as appropriate with a second-order Butterworth filter passed both forward and backward to avoid phase shifting based on the indicated period (T). Percentages are relative to the total variance observed in the time series where the two time-gaps have been filled via simple linear interpolation.

Time scales	Percentage of total variance
High frequencies ($T<2$ months)	37
Subannual frequencies ($2<T<11$ months)	36
Annual frequencies ($11<T<13$ months)	1
Interannual frequencies ($T>13$ months)	26

Integrating the absolute transport horizontally across the overlapping spans and vertically between 800 and 4800 dbar finds good agreement (Fig. 6). The correlation coefficient between the two absolute transport time series is very high ($r=0.96$), and the root-mean-squared (rms) difference is small (6 Sv) compared to the observed variability (Fig. 6). The correlation coefficient between the PIES and DHM relative transports using an 800 dbar level of no motion, i.e. those which have not been referenced using the bottom pressure, is similarly good at $r=0.91$. The standard deviation of the differences in relative transports is slightly larger at about 11 Sv, likely due to the sensitivity of the relative transport calculation to the vertical shear of the horizontal velocity right at the arbitrarily chosen 800 dbar reference level. Using a bottom reference level rather than 800 dbar produces a smaller standard deviation of the PIES vs. DHM relative transport difference (6 Sv) but also a lower correlation ($r=0.61$). Because the relative transport differences are difficult to meaningfully constrain, given the reference level issue, and because absolute transports are most relevant in the scope of this study, we will focus on the latter.

Given reasonable estimates of the accuracy of the absolute transport estimated via the PIES technique (~3–4 Sv; Meinen et al., 2004) and via the DHM technique (~4–5 Sv over the full water column, roughly 2–4 Sv in the DWBC layer; Johns et al., 2005) the observed absolute transport differences between the PIES and DHM estimates are roughly equivalent to the combined expected error bars. However, as noted above, the bottom pressure records used for referencing the relative velocity profiles (for both the DHM and the PIES) are identical here, having been built by combining the best pressure data at these two sites from the BPR data and the PIES pressure records. As such, ideally the 'error bars' for this comparison should be based solely on the estimated accuracies of the relative velocity profiles themselves. The accuracy for the PIES relative transports has previously been estimated as ~3 Sv (Meinen et al., 2004), while for the DHM the relative transport accuracy has previously been estimated as ~2 Sv (Johns et al., 2005). These error bars still (in combination) roughly equal the observed differences in absolute transport (~6 Sv), suggesting that the two systems (DHM+BPR and PIES) are producing equivalent absolute volume transports.

3.3. Transport variability between mooring spans

Transport variability in the DWBC layer between the WB-2 and WB-3 moorings has a peak-to-peak range of about 60 Sv, while the B-to-C, C-to-D, and D-to-E pairs of PIES[4] all encompass transports that vary within a peak-to-peak range of roughly 80–150 Sv, with the largest peak-to-peak transport range in the D-to-E span (Fig. 7). The transport in the small domain between the shelf and the WB-2 mooring has been estimated using four current meters on the WB-2 mooring, and the transport estimated in this manner is quite small (Fig. 7—top), rarely exceeding 1–2 Sv. The WB-2 to WB-3 and the B-to-C transport records are not correlated significantly with one another over this five-year period, nor are the B-to-C and C-to-D transport records (correlation coefficient $|r|<0.05$). There is some suggestion of anti-correlation between the C-to-D and D-to-E transport records, however while the correlation coefficient ($r=-0.50$) is significant at the 99% confidence level, the linear correspondence explains only 25% of the observed variance. To determine the significance of the time series correlations, we note that the integral time scale (e.g. Emery and Thomson, 1997; Tennekes and Lumley, 1972) of these transport records is approximately 30 days, and as such the records have roughly 30 degrees of freedom. This anti-correlation is to be expected, as the D site has long been identified as the 'time-mean' outer edge location of the DWBC (e.g. Bryden et al., 2005a; Lee et al., 1996). Meandering onshore and offshore of the DWBC would thereby cause an anti-correlated variability between the transports calculated in these two spans. An alternative interpretation is that when the DWBC increases, the recirculation offshore also increases. Although this interpretation cannot be excluded with these data, it is a less convincing one because one would expect some non-zero time lag between the increase in DWBC transport and the increase in the recirculation. The correlation would then be lagged, while a meandering effect would lead to a zero-lag correlation. Since there is no evidence of a lagged correlation in the data, the meandering interpretation seems more likely.

[4] Recall that PIES Site B is collocated with DHM Site WB-3 and PIES Site E is collocated with DHM Site WB-5.

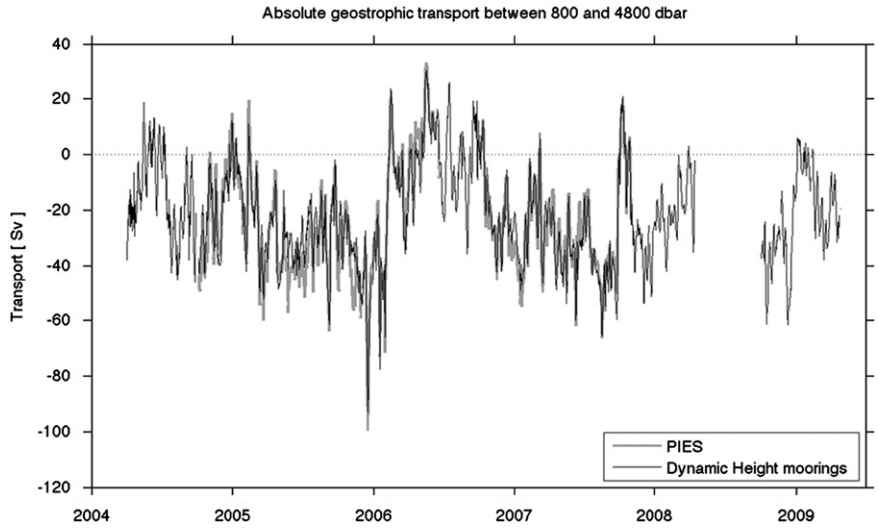

Fig. 6. Meridional absolute transport integrated between 800 and 4800 dbar between the DHM/PIES at sites WB-3/B and WB-5/E (black/gray lines, respectively). See Table 1 and/or Fig. 2 for locations.

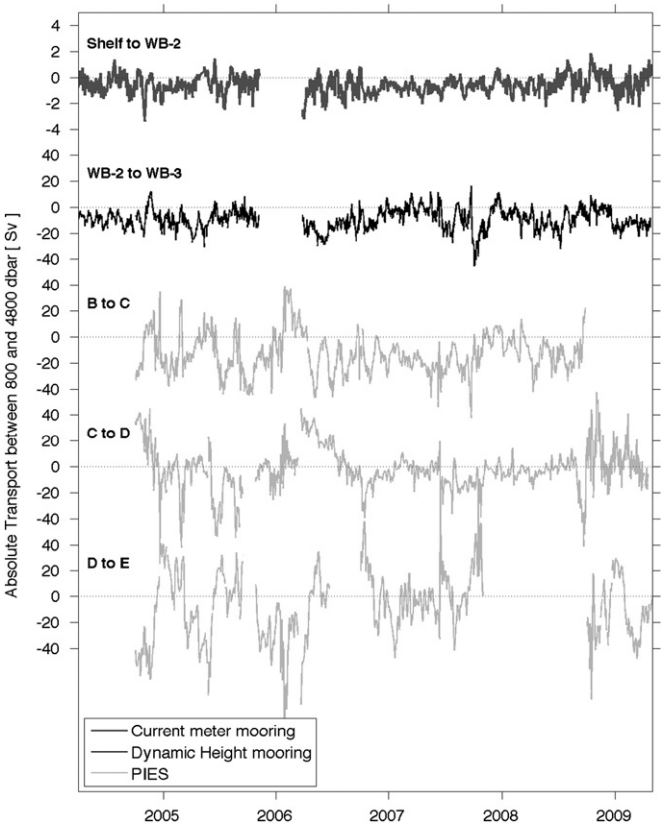

Fig. 7. Time series of absolute geostrophic transport integrated between 800 and 4800 dbar (or the bottom) and between the indicated pairs of DHM (black line) or PIES (light gray lines). Thick dark gray line indicates the small transport (notice the different transport scale) estimated between the shelf and the WB-2 mooring using current meters on the WB-2 mooring. Gaps indicate instrument failure at one side or the other.

3.4. Mean and variability of the DWBC transport

The transport of the DWBC in this region has historically been determined by integrating offshore from the continental slope until the sign of the transport changes, indicating the boundary between the DWBC and an offshore northward recirculation cell. This recirculation cell has long been hypothesized based on the unexpectedly large southward DWBC transport of ~35–40 Sv found at this location in both Eulerian and Lagrangian studies (e.g. Bryden et al., 2005a; Lee et al., 1996; Riser et al., 1978). The 'canonical' view of the DWBC and the MOC overall is that the net southward flow of NADW is of order 18–20 Sv (e.g. Cunningham et al., 2007; Lumpkin and Speer, 2007), so the remaining 15–20 Sv observed flowing southward in the DWBC at 26.5°N must recirculate northward somewhere offshore. The location of the E site (and the WB-5 site) was selected based on previous observations that suggested that the D-to-E span contains a significant fraction of this recirculation (Bryden et al., 2005a), and as such integration from the continental slope (essentially the WB-2 site) out to the E site (or WB-5) would yield a closer approximation of the 'through-put' transport of the DWBC at this latitude. Therefore, for the purposes of this paper, the DWBC transport will be defined as the total absolute transport integrated between 800 and 4800 dbar and from the continental shelf out to Site E/WB-5. Where appropriate, however, similar estimates of transport integrated only out to Site D will also be presented.

The variability of the DWBC defined out to Site E/WB-5 in this manner is quite high (Fig. 8), with a standard deviation (STD) of 16 Sv and a peak-to-peak range from −72 Sv to +14 Sv (negative indicating southward flow).[5] This is close to the 18 Sv STD found by Lee et al. (1996) using ~6 years of current meter data integrating from the shelf out to Site D in the late 1980s–early 1990s.[6] The mean southward DWBC transport of 32 Sv (±3 Sv; statistical standard error of the mean) integrated out to Site E/WB-5 found here should be viewed with some caution due to the issues raised earlier regarding the application of the time-mean near-bottom velocities used in creating the absolute velocity profiles. It is larger than the −27 Sv mean transport from the shelf to Site E/WB-5 estimated by Bryden et al. (2005a) as well as

[5] The mean transport integrated out to Site D, which has a few additional time gaps in the record due to instrument failures at Site D, was −29 Sv, while the standard deviation was 22 Sv and the observed range was from 105 Sv southward to 56 Sv northward.

[6] Note that Lee et al. (1996) subsequently excluded segments of their record when they believe the DWBC had meandered offshore of Site D and recalculated their standard deviation as 13 Sv from this subsampled time series—no similar subsampling was done here, so the 18 Sv standard deviation for their full period is what is cited here.

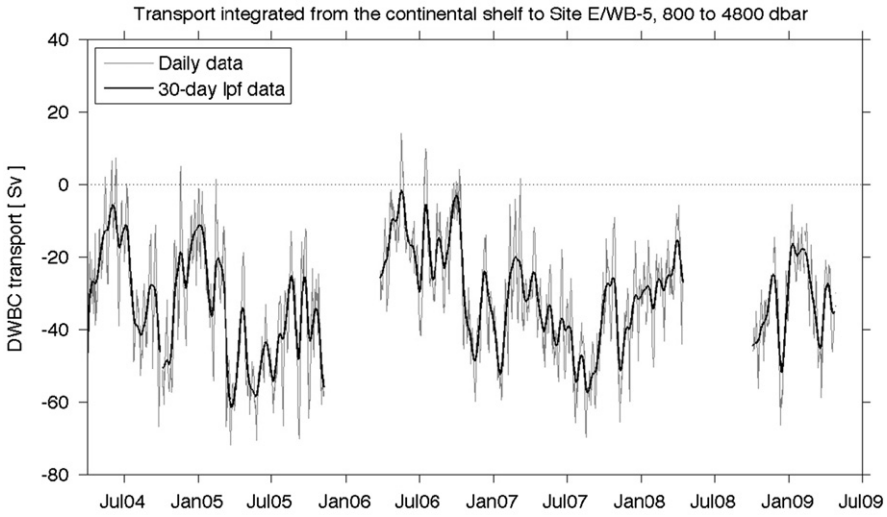

Fig. 8. Time series of absolute geostrophic transport of the DWBC integrated between 800 and 4800 dbar (or the bottom) and between the continental shelf and Site E/WB-5. Both the 'raw' 72-h low-pass filtered daily transport (gray) and the 30-day low-pass filtered data (black) are shown.

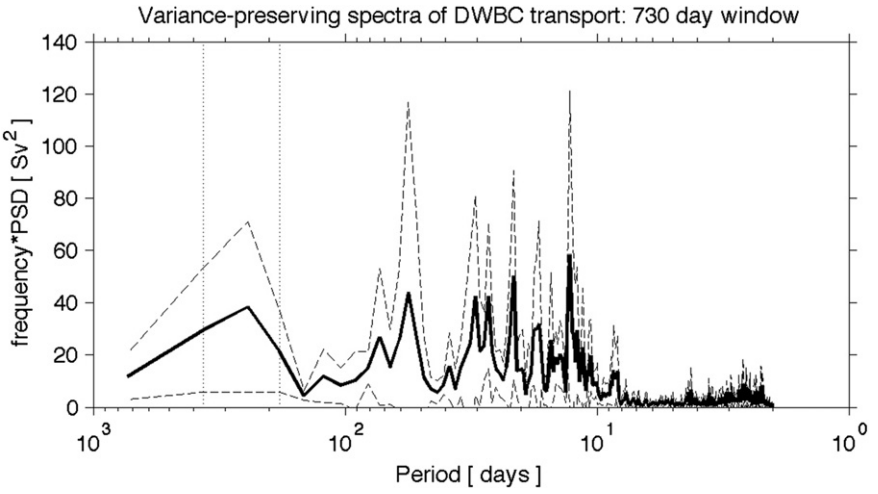

Fig. 9. Variance-preserving spectra of the DWBC transport integrated from 800 to 4800 dbar (or the bottom) and from the continental shelf out to Site E/WB-5. Thin dashed lines represent the 95% confidence limits. Vertical dotted lines indicate the annual and semiannual periods.

the estimate of −27 Sv derived from the first year of the DHM data (Johns et al., 2008). However, it should be borne in mind that each of these earlier estimates also suffers from significant uncertainties in the mean transport, due to the sparse sampling by current meters in the case of Bryden et al. (2005a), and to uncertainties in referencing of DHM transports (and only a 1 year long record) in the case of Johns et al. (2008). Our estimated transport out to Site D is −31 Sv,[7] which is smaller than the estimate of −35 Sv by Bryden et al. (2005a). Thus, for the 5-year period from 2004 to 2009, we find a slightly lower average southward DWBC transport close to the western boundary and little evidence of a significant offshore deep recirculation between Sites D and E/WB-5.

Variability exists on a wide range of time scales from a few days to more than a year, with perhaps the largest change being the transition from southward transports of less than 20 Sv in Spring–Summer 2006 to southward transports of 50–60 Sv in Summer–Autumn 2007 (Fig. 8). Spectral analysis of the time series is complicated by the two large gaps in the record due to the failure of the WB-2 mooring in late 2005–early 2006 and the loss of the Sites E and Site WB-5 bottom pressure data in mid 2008. Calculating the spectra after a simple linear interpolation of those two large gaps (and a few shorter gaps) finds significant variability at 12, 21, ~30, 55 and a fairly broad peak at ~230 days (Fig. 9). The ~30 days and ~230 days fluctuations are fairly consistent with the current meter observations from the 1980–1990s (Lee et al., 1996); however, the earlier mooring data did not consistently show the strong 12- and 21-day signals found here.

One of the key results of earlier studies was the discovery of annual and semiannual energy in the DWBC transport and the relatively good agreement between the observed annual cycle and that predicted by simple wind-driven models (Lee et al., 1996; Rosenfeld et al., 1989). Kanzow et al. (2008) suggested this seasonal variability could be the result of Rossby wave signals driven by seasonal Sverdrup transport variability. The earlier Lee et al. (1996) array found a maximum southward transport anomaly of nearly 15 Sv in October, with a northward maximum anomaly of about 8 Sv in February. A semiannual component of the signal led to smaller southward and northward anomaly maxima in April and June, respectively. The spectra of the modern transports (Fig. 9) suggest relatively little energy at annual or

[7] Note that due to time gaps in the different records, the averaging period for this calculation is not the same as that used for the −32 Sv determined from the full record for the integration from the coast out to Site E; the corresponding coast-to-Site E integrated using the same shorter time period is −35 Sv.

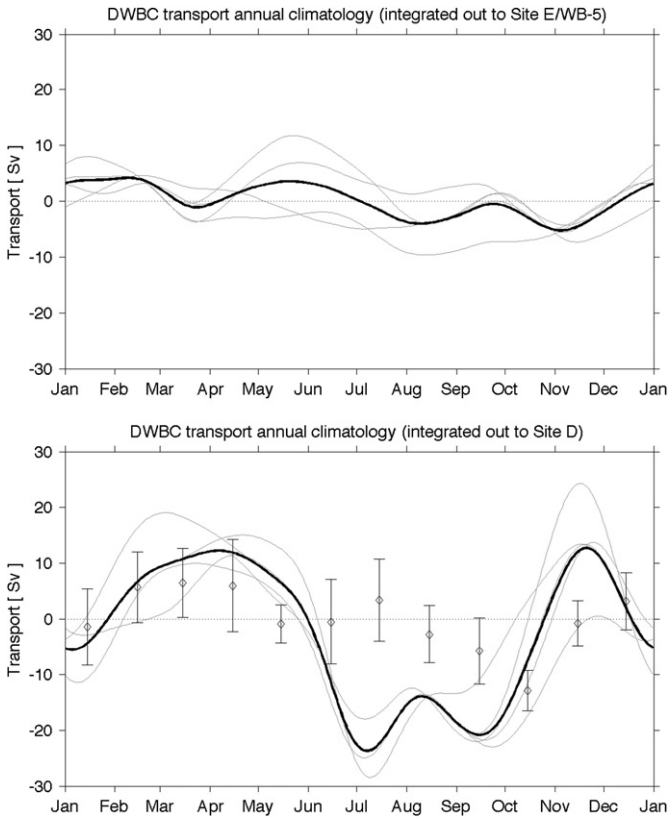

Fig. 10. Annual climatology of the absolute geostrophic transport calculated between 800 and 4800 dbar (or the bottom). Lateral integration boundaries are between the continental shelf and Site E/WB-5 (top panel) and between the shelf and Site D (bottom panel). Climatologies are determined using all five years of data (black line). Also shown are climatologies using Monte Carlo-style random selections of four years to illustrate statistical stability. In all cases the climatology is determined on a daily basis and the resulting data is smoothed with a 90-day lowpass filter to focus on the appropriate time scales. Also shown on the lower panel are the estimated annual climatology (diamonds) and the estimated error bars from the earlier current meter moorings—these are updated from the Lee et al. (1996) study by including additional data from 1996 to 1997.

semiannual periods, and the determination of an annual climatology, where the transport has been integrated out to Site E/WB-5, leads to a rather different picture than the earlier studies (Fig. 10, top). The first result that is evident is that the annual climatology is quite different depending upon whether it is determined using various subsets of four years of the data or all five years of data. In particular the annual climatologies look nothing alike other than suggesting a weak minimum in southward transport in February and a weak maximum in November. The annual climatology found here also has maximum amplitudes of ~5 Sv, a factor of 2–3 smaller than that found in the late 1980s and early 1990s by Lee et al. (1996).

It should be stressed, however, that the Lee et al. (1996) annual climatology was determined using data integrated only from the shelf out to Site D. An annual climatology calculated instead using the modern transports integrated out only to Site D in order to focus more on the near boundary flows yields an annual cycle with a much larger amplitude. This annual cycle is still very dependent on which subsets of years are used, however, and it is also still different from the Lee et al. (1996) climatology (Fig. 10, bottom). Note that the Lee et al. (1996) data plotted here (Fig. 10, black diamonds in bottom panel) has been updated with an additional ~18 months of current meter data from 1996 to 1997 that was not included in the original study. The peak-to-peak range of the modern 5-year annual climatology integrated out to Site D is nearly 40 Sv, with a maximum southward transport anomaly of nearly 25 Sv in July–September and a broad northward maximum flow anomaly of around 12 Sv in March–April. The updated Lee et al. (1996) results yield a very different annual climatology (Fig. 10) with a peak to peak range of about 19 Sv and a maximum (minimum) southward transport in October (March) of −13 Sv (+7 Sv). As noted in the Lee et al. (1996) paper, there is a suggestion of semiannual energy, with smaller maxima of northward and southward flow in November and January, respectively. However again the phasing of the annual cycle in the modern record is quite different than was found in the 1987–1997 current meter data. The 10–20 Sv differences observed between the annual climatologies using different subsets of four years versus the full five years illustrates the statistical 'tenuousness' of these signals (e.g. the differences between the black and gray lines in Fig. 10). Essentially none of these annual climatologies are statistically robust at a 95% confidence level (generally not even at a 67% confidence level, such as that estimated from the 1987 to 1997 current meter data in Fig. 10, where the transport climatology is only significantly different from zero, at the one standard error level, during the month of October).

The annual cycle found herein represents only ~1% of the total variance in the DWBC transport when integrated out to Site E/WB-5 (and only ~30% when transport is integrated only out to Site D) (Table 2). High frequency (periods < 2 months) and subannual frequency (periods of 2–11 months) variability each represent just over one-third of the total variance. As such it is difficult to extract a meaningful annual cycle without the aliasing of other time scales overwhelming the true signal. Interannual variability appears to represent just over a quarter of the total variance, but with only a five-year record this result may not be representative of a long-term truth. These percentages are somewhat different for the transport integrated only out to Site D, with nearly 50% of the total variance in transport out to Site D occurring at interannual periods and only ~15% occurring at periods less than two months (the rest being either annual or near semi-annual). However the large 10+ Sv differences between the gray lines and the black line in Fig. 10 (lower panel) still indicate that the annual cycle in transport integrated out only to Site D calculated with only 4–5 years of data is not particularly robust. Future work with longer records will be crucial for better understanding of the temporal distribution of energy in the DWBC transport variability.

Perhaps the most interesting result from the annual climatologies is the difference between the annual climatologies integrated out to Site D versus that integrated out to Site E/WB-5. Lee et al. (1996) hypothesized, based on their current meter data and the Anderson and Corry (1985) two-layer model results, that the annual cycle in circulation east of Abaco would be balanced by a broad-scale return circulation in the interior reaching out nearly to the Mid-Atlantic Ridge (MAR), effectively representing a barotropic 'topographic Sverdrup' response to the annual wind forcing (see Fig. 3 in Anderson and Corry, 1985). The results here suggest that the annual transport variability in the DWBC is compensated much closer to the western boundary, such that the streamlines of return flow would be squeezed primarily between Sites D and E/WB-5. This implies that the circulation associated with the annual cycle in this region is much more tightly controlled by the local topography than has previously been thought; however, future numerical modeling studies and/or more detailed field programs with more latitudinal extent will be required in order to fully understand the details of this circulation.

3.5. Implications of the observed DWBC transport variability

Many facts about the structure and phasing of DWBC transport fluctuations can be addressed with the time series described

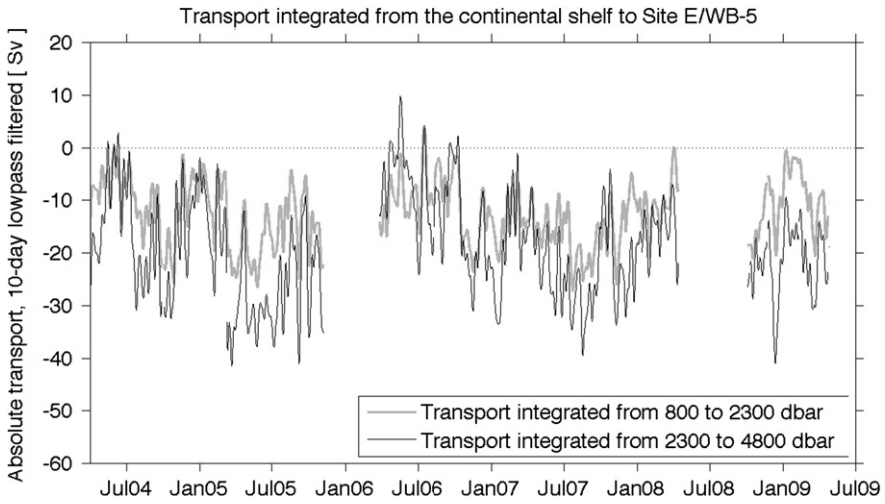

Fig. 11. DWBC transport (10-day low-pass filtered) broken into flow above 2300 dbar (gray line) and below 2300 dbar (black line). This pressure surface is roughly the mean separation between Labrador Sea Water above and Denmark Straits and Iceland-Scotland overflow waters below.

herein. Consider first the vertical distribution of the DWBC flow, here using the DHM data. Historical hydrographic studies along this line have demonstrated that at this latitude the upper waters of the DWBC that originate in the Labrador Sea are typically found above ~2300 dbar, while the deeper DWBC waters that originate at the Denmark Straits and Iceland–Scotland overflows are generally found below 2300 dbar (e.g. Molinari et al., 1998; van Sebille et al., 2011). Splitting the DWBC flow in this manner demonstrates that there are times when the upper DWBC waters are varying differently than the lower DWBC. For instance during January–February 2009 the upper DWBC has a minimum or even zero southward transport (note that the pressure leveling problem associated with determining absolute transports could lead to a bias in the mean transport) while the lower DWBC waters continue to flow southward (Fig. 11). Another uncorrelated "event" distinguishing upper DWBC from lower DWBC was found in an earlier analysis of the first year of data from the DHM data where the lower DWBC ceased while the upper DWBC continued (Johns et al., 2008). There is in general no clear indication of 'compensation' between the flows, i.e. increases in one layer that offset decreases in the other, and there is no statistically significant trend in either transport over the five year record. Despite these isolated 'events' the upper DWBC and lower DWBC transport time series are positively correlated ($r \sim 0.75$). This is consistent with earlier studies that have pointed to the barotropic nature of the flows in the DWBC off Abaco (e.g. Hacker et al., 1996). In fact, for a range of different layer separation pressure surfaces between 2000 and 3500 dbar the transports in the two layers are fairly highly positively correlated.[8] This suggests that while some of these fluctuations can be connected to density surface changes between the layers, such as the November 2004 example discussed in detail by Johns et al. (2008), many other events are probably unrelated to water mass/thermohaline forcing and are primarily related to locally and non-locally forced wind-driven events (e.g. Rossby waves). This also suggests that it is likely that using a density surface to separate the upper and lower DWBC is unlikely to significantly alter the conclusions presented here. An additional study is presently underway seeking to more fully identify the mechanisms behind the observed DWBC fluctuations using an augmented array including two additional sites between Sites D and E that were in the water from September 2006 to September 2008. Results from that research will be the basis for a future paper.

The observed variability of the DWBC transport (STD ~ 16 Sv) is significantly higher than that of the basin-wide MOC transport (STD ~ 5 Sv) determined via integration of the meridional velocity in the upper water column from Florida to Morocco above the basin-wide flow reversal at roughly 1000 dbar (see Kanzow et al., 2010, for the details of the MOC calculation). This suggests that the deep fluctuations observed along the western boundary must be partially compensated by counter-flows to the east of Site E/WB-5. Because the complete trans-basin array involves moorings on either side of the MAR (see Fig. 1), the transport between Site E/WB-5 and the mooring on the western side of the ridge (MAR-W) can be determined in the same manner as has been described previously (Fig. 12).[9] Evaluating the transport records together it is clear that a significant component of the DWBC transport integrated out to Site E/WB-5 is compensated by opposing flows between Site E/WB-5 and MAR-W.[10] The two records have a moderately strong anti-correlation ($r = -0.79$) with the daily data, and an even higher anti-correlation for the 30-day low-pass filtered records ($r = -0.84$). Combining the two to produce an estimate of the transport from the Bahamas to the western flank of the MAR eliminates the compensating component of the transport and yields the net deep flow between 800 and 4800 dbar and between the continental shelf and the MAR (Fig. 12, bottom line). There is still significant variability in this transport (STD of 10 Sv for daily data; 7 Sv for 30-day low-pass filtered data), and this variability is about twice that of the total MOC. The range of the deep flow integrated from the shelf to MAR-W extends from a minimum southward flow of 6 Sv to a

[8] Comparison of transports integrated from Site B/WB-3 to Site E/WB-5 using either the PIES or the moorings separately finds very similar results for the upper and lower DWBC flows (not shown). The two estimates of the lower layer DWBC flow are very highly correlated ($r \sim 0.99$) regardless of the layer separation pressure selected, and correlations of the two estimates of the DWBC flow in the upper layer are quite high also ($r \sim 0.88$–0.92).

[9] Note that essentially no information is available on the time mean near-bottom flow for the full span between Site E/WB-5 and MAR-W, and as such there is no time-mean bottom velocity to add to the gradient of the bottom pressure gauges in that span. For the purposes of this study the time-mean deep flow in that large span is assumed to be zero—therefore the transports integrated from Site E/WB-5 to MAR-W and from the Shelf to MAR-W transports should be considered anomalies only, with focus placed on the time variability of the signal and not on the time-mean.

[10] Note that in some other publications this site is denoted as "MAR-1", however here we are adopting the "MAR-W" notation as it is more descriptive.

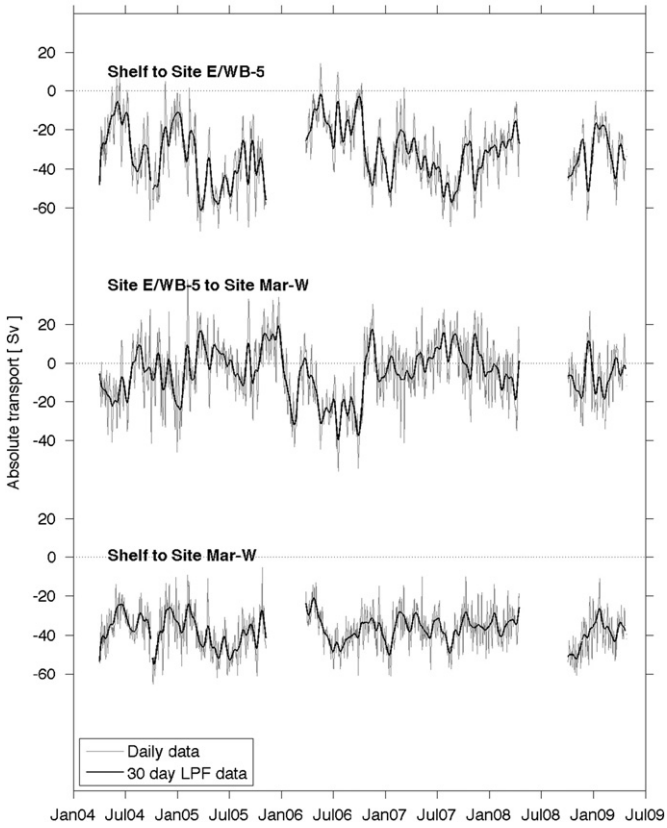

Fig. 12. Absolute geostrophic transport estimated between 800 and 4800 dbar (or the bottom) and in the indicated spans between moorings. Both daily data (gray) and 30-day low-pass filtered data (black) are shown; gaps indicate instrument failures. Note that due to the lack of time-mean velocity information in the Site E/WB-5 to Mar-W span for leveling the bottom pressure data, the lower two lines may have an unknown mean offset.

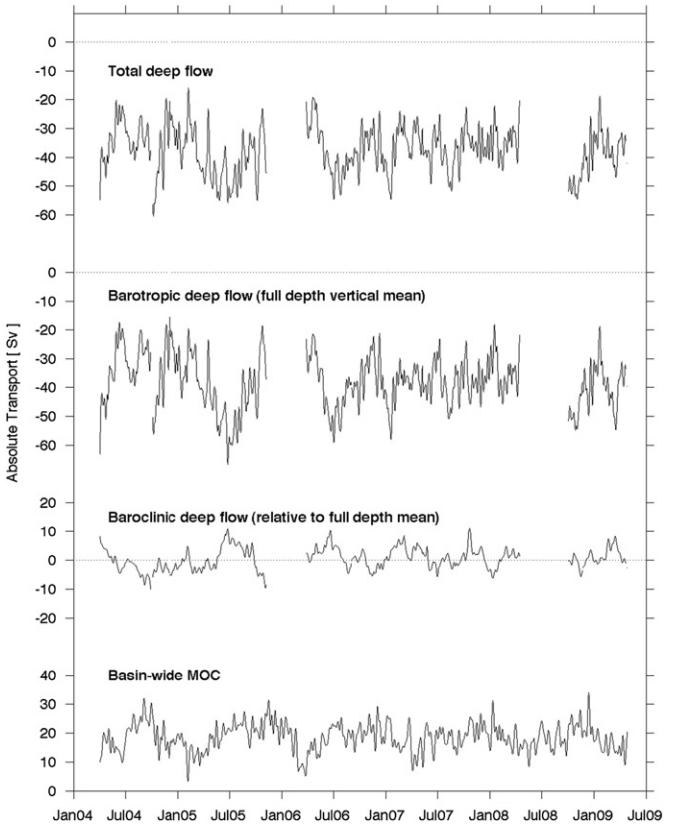

Fig. 13. Deep transport in the western basin, integrated from the shelf to MAR-W, plotted as the total transport, the barotropic transport (defined based on a full-depth vertical average), and the baroclinic transport (defined as the difference from the full-depth vertical average). Also shown is the basin-wide MOC upper-ocean transport from the basin-wide array as calculated by Kanzow et al. (2010). All records have been smoothed with a 10-day low-pass filter.

maximum southward flow of 66 Sv. Analysis of the trans-basin mooring data has previously suggested that MOC transport variability integrated to the MAR can be much larger than that integrated across the basin, due to eddies and Rossby waves (Bryden et al., 2009; Kanzow et al., 2008, 2009). The results presented herein clearly demonstrate that these signals have strong representations in the deep layer and must involve flow that exists on both sides of the MAR (i.e. it is likely more complicated than just local eddies and Rossby waves).

The variability in the shelf to MAR-W deep transport occurs over essentially the same time scales as the shelf to Site E/WB-5 transport. Transport changes greater than 20 Sv occur over time scales of a few days to months. The hypothesis that the shorter-period fluctuations (periods of a few days to weeks) are barotropic signals with short horizontal scales (e.g. Johns et al., 2008) can be evaluated by separating the absolute transports into barotropic and baroclinic components (Fig. 13). The barotropic flow is defined as the vertical mean from the surface to the ocean bottom, while the baroclinic flow is the fluctuation about this vertical mean. Note that because transports herein are integrated only from 800 to 4800 dbar (or the bottom), while the barotropic flow is defined to be vertically-averaged over the full water column, the baroclinic flow in the deep layer will generally have a non-zero transport. The variability of the total deep flow is highly correlated to the barotropic flow ($r=0.93$) while there is no meaningful correlation to the baroclinic flow ($r=-0.09$). The barotropic and baroclinic components are weakly anti-correlated with one another ($r=-0.44$), which is statistically significant at the 95% level (based on ~30 degrees of freedom in the records described earlier where the integral time scale is ~30 days and two integral time scales are needed for each degree of freedom). Not surprisingly the bulk of the variability in the deep transport is related to the barotropic component, with the STD of the barotropic and baroclinic transports being 11 Sv and 4 Sv, respectively. The fact that the barotropic STD exceeds that of the total transport indicates some degree of compensation, consistent with the weak anti-correlation noted earlier. The weak anti-correlation also indicates the existence of a mixed barotropic/baroclinic mode of variability as has been suggested by Bryden et al. (2009).

In principle the deep flow must balance the northward upper flow of the MOC in some manner to conserve mass (neglecting the small ~1 Sv flow through the Bering Straits). However, while there is a tendency for negative correlation, neither the total transport nor the barotropic or the baroclinic components of the deep transport in the western basin is significantly correlated with the MOC for any lag/lead (respectively $r=-0.33$, -0.24 and -0.13 for zero lag). The amplitude of the deep baroclinic transport (4 Sv) is roughly comparable to that of the MOC (5 Sv), but its correlation is actually weaker than that of the total transport. Two obvious limitations of the deep integral done here are that it neglects the flow below 4800 dbar, and that the upper ocean MOC calculation is made above a moving basin-wide transport inflection point (e.g. Cunningham et al., 2007) rather than above a fixed pressure surface of 800 dbar such as is used here. The vertical extent of both of these layers at the top and bottom of the integration domain are only ~100–400 m, and as such it is unlikely that sufficient transport can flow through those layers to truly reduce the observed deep absolute transport variability

down to the observed level of the MOC (very broad horizontal-scale velocities on the order of $10+$ cm s^{-1} would be required). For example, recently published research using additional moorings deployed in the deep layer has estimated that the flow below 4800 dbar has variations of only $\sim$1 Sv (Frajka-Williams et al., in press). Therefore the results presented herein are not sensitive to the details of the upper and lower integration limits. This suggests both that local processes are quite significant in the western basin transport, and that some component of the deep signal must be occurring in the eastern basin and compensating for the observed western basin flows despite the lack of connection between the two deep basins at this latitude.

4. Conclusions

The strong DWBC transport variability observed during 2004–2009, and the significant variability that still exists in the deep ocean even when integrated across the entire western basin out to the MAR, demonstrates clearly that the deep layer is more energetic than has previously been thought and that the MOC is a complicated system. Attribution of observed MOC variability will require detailed horizontal and vertical resolution information across the basin. The five years of PIES and DHM data presented herein lead to several important conclusions about the variability of the DWBC and MOC as well as future observing systems for these key circulation features.

The water-mass variability observed using the DHM (and to a lesser extent the PIES) demonstrates that even in this highly-sampled region of the ocean (30+CTD sections in the past $\sim$30 years) the collection of snapshot sections can still significantly underestimate the total range of variability the ocean is exhibiting. Without continuous measurement systems such as the moored array at 26.5°N, the possibility for aliasing of strong but short-lived hydrographic anomalies (e.g. the $\sim$5 °C, 1 psu event in May–June 2006 at Site E/WB-5) into apparent long-term trends will be significant.

The five-year DHM and PIES records presented herein demonstrate strong volume transport variability at both the shortest periods (5–80 days) and the longest periods (greater than 400 days), with very little energy present at semi-annual or annual periods. This lack of annual and semi-annual energy is surprising in light of earlier current meter mooring records in the same region (e.g. Lee et al., 1996), and the results here demonstrate that the stream-function field for the annual and semi-annual flows must be much tighter to the coast than has previously been suspected. This calls into question the basic dynamics of the annual cycle of deep flow, as predicted by Anderson and Corry (1985), and implies stronger local topographic control of the circulation. This, in turn, has important implications for understanding observed DWBC variability both here and at other isolated single-latitude or single-line arrays. Additional meridional resolution in these observing arrays may be required, near the western boundary at least, in order to best interpret the observed signals.

It is also clear from the results presented herein that the flow in the deep basins on either side of the Mid-Atlantic Ridge must have some anti-correlation to account for the variability in the flow in the western basin greatly exceeding (by $\sim$100%) the variability of the total MOC. While the array in the western basin could benefit from better horizontal resolution to understand more details of the recirculation cell in that basin, it is also clear that the existing portion of the trans-basin array that is east of the MAR does not have sufficient resolution to do a similar analysis to that done here (i.e. it cannot evaluate the horizontal structure of the flow near the boundary nor can it distinguish basin interior flow from flow along the boundary). Assuming a perfect anti-correlation in the western and eastern basins, and the requirement that the basin-wide deep layer flow must match the basin-wide upper layer flow, the deep transport variability in the eastern basin would have a standard deviation of roughly 8 Sv. Based on the results presented here, it is evident that better resolution, particularly in the horizontal, is required to understand the deep transport variability in the two sub-basins and better attribute the observed MOC signals.

Acknowledgments

The authors wish to express their appreciation and admiration to Tom Rossby, who was heavily involved in the invention of some of the scientific instruments used herein, who served on some of our dissertation committees, who taught some of our graduate school classes, and who has been a tireless advocate for observational physical oceanography for many years while simultaneously being a great colleague. Thank you Tom! The authors would also like to express their appreciation to the ship officers and crew of the RRS Discovery, R/V Seward Johnson, R/V Knorr, R/V Oceanus, R/V Cape Hatteras, and the NOAA Ship Ronald H. Brown for their assistance in maintaining the Deep Western Boundary Current components of these joint arrays. Support for this program was provided by the NOAA Climate Program Office, the NSF Physical Oceanography Program, and the NERC Rapid Climate Change Program. Thanks also for the outstanding contributions of the project teams at the Atlantic Oceanographic and Meteorological Laboratory, at the University of Miami, and at the National Oceanography Centre. Very helpful comments on improving an earlier draft of this manuscript were kindly provided by Libby Johns, Lisa Beal and two anonymous reviewers.

Appendix A. Pressure drift removal and record merging

Bottom pressure measurements are essential to obtaining absolute velocity profiles, however there are some particular difficulties in creating long-term records from subsequent deployments of bottom pressure recording instruments. The first well-known challenge is that the tide signals in bottom pressure records exceed by roughly an order of magnitude the desired signals associated with deep geostrophic currents of interest to this type of study. Careful removal of these tides is essential to avoid aliasing any residual energy into the longer-period time scales of interest (Watts and Kontoyiannis, 1990). A larger challenge comes from the fact that all bottom pressure sensors experience drift that is unrelated to the physical ocean currents. These drifts typically take the form of a linear record-length drift as well as an exponential drift over the first few months of the record (e.g. Donohue et al., 2010; Watts and Kontoyiannis 1990). Amplitudes of these drifts are typically on the order of 0.1–0.3 dbar, which is quite significant as the ocean signals of interest (after removal of the tides) are a factor of 2–5 smaller than the drifts (Fig. A1). The exponential component of the drift appears to be lessened in many cases by pre-pressurizing the sensors for a few months prior to deployment (Watts and Kontoyiannis, 1990); however, this does not appear to significantly decrease the linear record-length trends. These record length trends have a significant implication in that when removing the trend one also removes any very long period signal that might be in the record (periods much longer than the record length such that they would appear as a linear drift). For that reason longer deployments of pressure sensors are better; for this program BPRs and PIES are generally planned with two or four

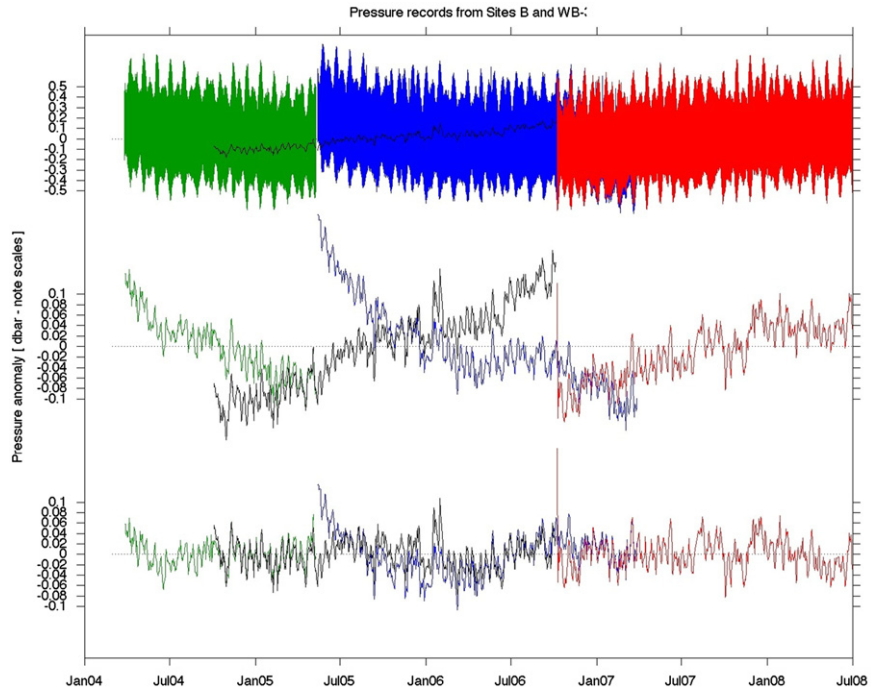

Fig. A1. Example illustrating the steps involved in combining overlapping pressure records as well as some of the challenges using four overlapping records from Sites B and WB-3. Upper lines: raw records from two bottom pressure recorders (green and blue), from one recovered PIES (red), and from one PIES acoustic telemetry record for an instrument that failed to surface on recovery (black). Raw records are half-hourly for bottom pressure recorders, hourly for the recovered PIES, and daily from the PIES telemetry record. Note the larger pressure scale on the upper lines. Middle lines: the same four records after passing them through a 72-h low-pass filter to remove the tides (the telemetry PIES record was filtered internally in the instrument prior to acoustic transmission and so was not filtered again here). Bottom lines: the same four records after the removal of a least-squares-fit linear record-length trend from each record.

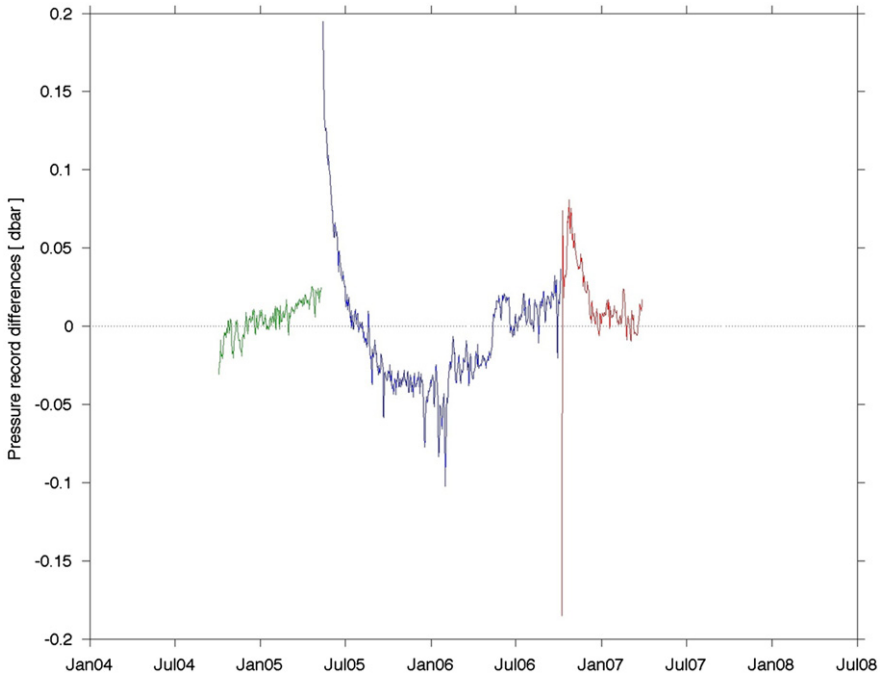

Fig. A2. Differences between the overlapping segments of the pressure records shown in the lower lines of Fig. A1.

year deployments, respectively. Drifts can also be better identified by doing overlapping deployments, which is being done for many of the sites in these programs.

The bottom pressure record from site B/WB-3 serves as an example, which was constructed using four overlapping records (Fig. A1). The steps in combining the records are as follows. First, one must remove the large signals associated with the tides (top lines in Fig. A1). The residual variability after the removal of the tides is about a factor of five smaller (note the different y-axis scales on the top and middle sets of records in Fig. A1). If one then removes a record length linear trend from the overlapping records one can view the overlapping segments and their

differences (Fig. A2) in order to evaluate the potential exponential drifts, and can determine the accuracy with which the linear drifts can be removed. In the example illustrated in Figs. A1 and A2, the agreement between the first PIES (black line in Fig. A1) and the first bottom pressure recorder (green line) is excellent, with the differences (Fig. A2) suggesting a small (0.01–0.02 dbar) difference in the record-length drifts removed in early 2005. The end of the record from the second bottom pressure record (blue line in Fig. A1) and the beginning of the second PIES record (red line) agree even better, with no indication of a linear drift difference in the 2007 data in Fig. A2. The differences between mid-2005 and the end of 2006 illustrate the significant exponential drift issues that can be exhibited by some sensors. In this example, the first PIES record was used throughout this period and the second bottom pressure recorder (blue line in Fig. A1) was not utilized. A comparison of overlapping records from Site E/WB-5 found similar differences in linear drifts of a few hundredths of a dbar and smaller exponential drifts (not shown). For the purposes of this study, it is estimated that the blended pressure data from consecutive overlapping records is accurate to within ~0.01–0.02 dbar for time scales of a year or greater, and at the full resolution of the pressure sensors themselves (~0.001 dbar) for time scales significantly shorter than a year.

References

Anderson, D.L.T., Corry, R.A., 1985. Seasonal transport variations in the Florida straits: a model study. J. Phys. Oceanogr. 15, 773–786.

Baringer, M.O., Molinari, R., 1999. Atlantic Ocean baroclinic heat flux at 24–26°N. Geophys. Res. Lett. 26 (3), 353–356.

Bower, A.S., Lozier, M.S., Gary, S.F., Böning, C.W., 2009. Interior pathways of the North Atlantic Meridional Overturning Circulation. Nature 459, 243–248, http://dx.doi.org/10.1038/nature07979.

Bryden, H.L., Johns, W.E., Saunders, P.M., 2005a. Deep Western Boundary Current East of Abaco: mean structure and transport. J. Mar. Res. 63, 35–57.

Bryden, H.L., Longworth, H.R., Cunningham, S.A., 2005b. Slowing of the Atlantic Meridional Overturning Circulation at 25°N. Nature 438, 655–657.

Bryden, H.L., Mujahid, A., Cunningham, S.A., Kanzow, T., 2009. Adjustment of the basin-scale circulation at 26°N to variations in Gulf Stream, Deep Western Boundary Current and Ekman transports as observed by the RAPID array. Ocean Sci. 5, 421–433.

Chave, A.D., Luther, D.S., Filloux, J.H., 1997. Observations of the Boundary Current System at 26.5°N in the Subtropical North Atlantic Ocean. J. Phys. Oceanogr. 27 (9), 1827–1848.

Cunningham, S.A., Kanzow, T., Rayner, D., Baringer, M.O., Johns, W.E., Marotzke, J., Longworth, H.R., Grant, E.M., Hirschi, J.J.-M., Beal, L.M., Meinen, C.S., Bryden, H.L., 2007. Temporal Variability of the Atlantic Meridional Overturning Circulation at 26.5°N. Science 317, 935, http://dx.doi.org/10.1126/science.1141304.

Dengler, M., Schott, F.A., Eden, C., Brandt, P., Fischer, J., Zantopp, R., 2004. Break-up of the Atlantic Deep Western Boundary Current into Eddies at 8°S. Nature 432, 1018–1020.

Donohue, K.D., Watts, D.R., Tracey, K.L., Greene, A.D., Kennelly, M., 2010. Mapping circulation in the Kuroshio extension with an array of current and pressure recording inverted echo sounders. J. Atmos. Oceanic Technol. 27, 507–527, http://dx.doi.org/10.1175/2009JTECHO686.1.

Emery, W.J., Thomson, R.E., 1997. Data Analysis Methods in Physical Oceanography. Pergamon Press, Oxford.

Frajka-Williams, E., Cunningham, S.A., Bryden, H., King, B.A. Variability of Antarctic bottom water at 26°N in the Atlantic. J. Geophys. Res., 116, C11026, http://dx.doi.org/10.1029/2011JC007168, in press.

Hacker, P., Firing, E., Wilson, W.D., Molinari, R., 1996. Direct observations of the Current Structure East of the Bahamas. Geophys. Res. Lett. 23 (10), 1127–1130.

Johns, E., Fine, R.A., Molinari, R.L., 1997. Deep flow along the Western Boundary South of the Blake Bahamas outer ridge. J. Phys. Oceanogr. 27 (10), 2187–2208.

Johns, W.E., Kanzow, T., Zantopp, R., 2005. Estimating ocean transports with dynamic height moorings: an application in the Atlantic Deep Western Boundary Current. Deep-Sea Res. I 52 (8), 1542–1567, http://dx.doi.org/10.1016/j.dsr.2005.02.002.

Johns, W.E., Beal, L.M., Baringer, M.O., Molina, J.R., Cunningham, S.A., Kanzow, T., Rayner, D., 2008. Variability of Shallow and Deep Western Boundary Currents off the Bahamas during 2004–05: results from the 26°N RAPID–MOC array. J. Phys. Oceanogr. 38, 605–623, http://dx.doi.org/10.1175/2007JPO3791.1.

Johns, W.E., Baringer, M.O., Beal, L.M., Cunningham, S.A., Kanzow, T., Bryden, H.L., Hirschi, J.J.-M., Marotzke, J., Meinen, C.S., Shaw, B., Curry, R., 2011. Continuous array-based estimates of Atlantic ocean heat transport at 26.5°N. J. Clim. 24 (5), 2429–2449, http://dx.doi.org/10.1175/2010JCLI3997.1.

Joyce, T.M., Dunworth-Baker, J., Pickart, R.S., Torres, D., Waterman, S., 2005. On the Deep Western Boundary Current south of Cape Cod. Deep-Sea Res. II 52, 615–625.

Kanzow, T., Johnson, H., Marshall, D.P., Cunningham, S.A., Hirschi, J.J.-M., Mujahid, A., Bryden, H.L., Johns, W.E., 2009. Basin-wide integrated volume transports in an Eddy-Filled Ocean. J. Phys. Oceanogr. 39, 3091–3110.

Kanzow, T., Send, U., Zenk, W., Chave, A.D., Rhein, M., 2006. Monitoring the integrated deep meridional flow in the Tropical North Atlantic: long-term performance of a geostrophic array. Deep-Sea Res. I 53, 528–546.

Kanzow, T., Cunningham, S.A., Rayner, D., Hirschi, J.J.-M., Johns, W.E., Baringer, M.O., Bryden, H.L., Beal, L.M., Meinen, C.S., Marotzke, J., 2007. Observed flow compensation associated with the meridional overturning at 26.5°N in the Atlantic. Science 317, 938, http://dx.doi.org/10.1126/science.1141293.

Kanzow, T., Send, U., McCartney, M., 2008. On the variability of the deep meridional transports in the Tropical North Atlantic. Deep-Sea Res. I 55, 1601–1623, http://dx.doi.org/10.1016/j.dsr.2008.07.011.

Kanzow, T., Cunningham, S.A., Johns, W.E., Hirschi, J.J.-M., Marotzke, J., Baringer, M.O., Meinen, C.S., Chidichimo, M.P., Atkinson, C., Beal, L.M., Bryden, H.L., Collins, J., 2010. Seasonal variability of the Atlantic Meridional Overturning Circulation at 26.5°N. J. Clim. 23, 5678–5698, http://dx.doi.org/10.1175/2010JCLI3389.1.

Larsen, J.C., Sanford, T.B., 1985. Florida Current volume transports from voltage measurements. Science 227, 302–304.

Leaman, K.D., Harris, J.E., 1990. On the average absolute transport of the Deep Western Boundary Currents East of Abaco Island, the Bahamas. J. Phys. Oceanogr. 20 (3), 467–475.

Lee, T.N., Johns, W., Schott, F., Zantopp, R., 1990. Western Boundary Current structure and variability East of Abaco, Bahamas at 26.5°N. J. Phys. Oceanogr. 20 (3), 446–466.

Lee, T.N., Johns, W.E., Zantopp, R.J., Fillenbaum, E.R., 1996. Moored observations of Western Boundary Current variability and thermohaline circulation at 26.5°N in the subtropical North Atlantic. J. Phys. Oceanogr. 26 (6), 962–983.

Lumpkin, R., Speer, K., 2007. Global Ocean meridional overturning. J. Phys. Oceanogr. 37 (10), 2550–2562, http://dx.doi.org/10.1175/JPO3130.1.

Meinen, C.S., Watts, D.R., 2000. Vertical structure and transport on a transect across the North Atlantic Current near 42°N: time series and mean. J. Geophys. Res. 105 (C9), 21,869–21,892.

Meinen, C.S., Garzoli, S.L., Johns, W.E., Baringer, M.O., 2004. Transport variability of the Deep Western Boundary Current and the Antilles Current off Abaco Island, Bahamas. Deep-Sea Res. I 51, 1397–1415.

Meinen, C.S., Baringer, M.O., Garzoli, S.L., 2006. Variability in Deep Western Boundary Current transports: preliminary results from 26.5°N in the Atlantic. Geophys. Res. Lett. 33, L17610, http://dx.doi.org/10.1029/2006GL026965.

Meinen, C.S., Baringer, M.O., Garcia, R.F., 2010. Florida current transport variability: an analysis of annual and longer-period signals. Deep-Sea Res. I 57, 835–846.

Molinari, R.L., 1986. Subtropical Atlantic climate studies (STACS) revisited. EOS 67 (5), 59–60.

Molinari, R.L., Maul, G.A., Chew, F., Wilson, W.D., Bushnell, M., Mayer, D., Leaman, K., Schott, F., Lee, T., Zantopp, R., Larsen, J.C., Sanford, T.B., 1985. Subtropical Atlantic climate studies: introduction. Science 227, 292–295.

Molinari, R.L., Fine, R.A., Johns, E., 1992. The Deep Western Boundary Current in the Tropical North Atlantic Ocean. Deep-Sea Res. 39 (11), 1967–1984.

Molinari, R.L., Fine, R.A., Wilson, W.D., Curry, R.G., Abell, J., McCartney, M.S., 1998. The arrival of recently formed Labrador Sea Water in the Deep Western Boundary Current at 26.5°N. Geophys. Res. Lett. 25 (13), 2249–2252.

Rayner, D., Hirschi, J.J.-M., Kanzow, T., Johns, W.E., Wright, P.G., Frajka-Williams, E., Bryden, H.L., Meinen, C.S., Baringer, M.O., Marotzke, J., Beal, L.M., Cunningham, S.A., 2011. Monitoring the Atlantic meridional overturning circulation. Deep-Sea Res. II. 48, 1744–1753.

Riser, S.C., Freeland, H., Rossby, H.T., 1978. Mesoscale motions near the Deep Western Boundary of the North Atlantic. Deep-Sea Res. 25, 1179–1191.

Rosenfeld, L.K., Molinari, R.L., Leaman, K.D., 1989. Observed and modeled annual cycle of transport in the straits of Florida and East of Abaco Island, the Bahamas (26.5°N). J. Geophys. Res. 94 (C4), 4867–4878.

Rossby, T., 1969. On monitoring depth variations of the main thermocline acoustically. J. Geophys. Res. 74 (23), 5542–5546.

Schott, F.A., Zantopp, R., Stramma, L., Dengler, M., Fischer, J., Wibaux, M., 2004. Circulation and deep-water export at the western exit of the Subpolar North Atlantic. J. Phys. Oceanogr. 34 (4), 817–843.

Schott, F.A., Dengler, M., Zantopp, R., Stramma, L., Fischer, J., Brandt, P., 2005. The Shallow and Deep Western Boundary circulation of the South Atlantic at 5–11°. J. Phys. Oceanogr. 35, 2031–2053.

Smith, W.H.F., Sandwell, D.T., 1997. Global sea floor topography from satellite altimetry and ship depth soundings. Science 277 (5334), l956–1962.

Stommel, H., 1957. A survey of ocean current theory. Deep-Sea Res. 4, 149–184.

Stommel, H., Arons, A.B., 1960. On the Abyssal circulation of the World Ocean—II. An idealized model of the circulation pattern and amplitude in oceanic basins. Deep-Sea Res. 6, 217–233.

Stouffer, R.J., Yin, J., Gregory, J.M., 2006. Investigating the causes of the response of the thermohaline circulation to past and future climate changes. J. Clim. 19 (8), 1365–1387.

Swallow, J.C., Worthington, L.V., 1961. An observation of a deep countercurrent in the Western North Atlantic. Deep-Sea Res. 8, 1–19.

Tennekes, H., Lumley, J.L., 1972. A First Course in Turbulence. The MIT Press. (300 pp.).

van Sebille, E., van Leeuwen, P.J., Biastoch, A., Barron, C.N., de Ruijter, W.P.M., 2009. Lagrangian validation of numerical drifter trajectories using drifting buoys: application to the agulhas system. Ocean Model. 29, 269–276, http://dx.doi.org/10.1016/j.ocemod.2009.05.005.

van Sebille, E., Baringer, M.O., Johns, W.E., Meinen, C.S., Beal, L.M., de Jong, M.F., van Aken, H.M., 2011. Propagation pathways of classical Labrador Sea Water fromits source region to 26°N. J. Geophys. Res. 116, C12027, http://dx.doi.org/10.1029/2011JC007171.

Vellinga, M., Wood, R.A., 2002. Global climatic impacts of a collapse of the Atlantic thermohaline circulation. Clim. Change 54 (3), 251–267.

Watts, D.R., Kontoyiannis, H., 1990. Deep-ocean bottom pressure measurement: drift removal and performance. J. Atmos. Oceanic Technol. 7 (2), 296–306.

Watts, D.R., Rossby, H.T., 1977. Measuring dynamic heights with inverted echo sounders: results from MODE. J. Phys. Oceanogr. 7, 345–358.

Watts, D.R., Sun, C., Rintoul, S., 2001. A two-dimensional gravest empirical mode determined from hydrographic observations in the Subantarctic Front. J. Phys. Oceanogr. 31 (8), 2186–2209.

Zhang, R., Delworth, T.L., 2006. Impact of Atlantic multidecadal oscillations on India/Sahel Rainfall and Atlantic Hurricanes. Geophys. Res. Lett. 33 (17), http://dx.doi.org/10.1029/2006GL026267.